Online Computation of the Stiffness Matrix in Robotic Structures Using Finite Element Analysis

TR-CIM-10-05 September 2010

Afshin Taghvaeipour, Jorge Angeles and Larry Lessard

Department of Mechanical Engineering and Centre for Intelligent Machines,
McGill University

Abstract

Finite Element Analysis (FEA) is known to be a highly reliable tool for structural analysis, but this is usually conducted offline. Online use of FEA is usually out of the question because it is highly demanding in terms of computing time. We show in this report how the Cartesian stiffness matrix of robotic structures of a certain class can be computed online with FEA support. The procedure is based on an extension of the concept of *generalized spring* that is capable of handling anisotropic linearly elastic structures. In this way, FEA is conducted offline, to compute the Cartesian stiffness matrix of a structural part of a complex shape. This matrix is then used to update the posture-dependent Cartesian stiffness matrix of the overall structure. As an illustrative example, the procedure is applied to a Schönflies motion generator that features two parallelogram linkages fabricated of carbon fiber. In order to illustrate the online feasibility of the computation involved, the root-mean square value of the eigenvalues of a dimensionless factor of the stiffness matrix is plotted along a standard trajectory adopted by the industry.

Contents

1 Introduction

The interaction of a robot with the environment brings about wrenches applied to its moving platform (MP). The flexible elements of the robot, if properly designed, allow for "small"-amplitude displacements (SADs) of the MP in response to the applied wrenches. In the case of robots designed for fast and accurate tasks, the calculation of these displacements is crucial, which calls for an *elastostatic analysis*. A SAD is understood here in the sense of screw theory [1], wherein a line is represented by a six-dimensional array of Plücker coordinates, of which only four are independent; a screw is then defined as a line array with a pitch, its fifth independent parameter. A sixth parameter, the amplitude A, multiplying the screw array then defines a twist—point velocity and angular velocity— or a wrench—force and moment—depending on whether A has units of angular velocity ω or of force F. If A is defined as $A = \omega\Delta t$, and the product $\omega\Delta t \ll 1$, then a SAD is obtained instead of the twist. Elastostatic analysis hinges on the stiffness matrix of the robotic structure. This analysis is mainly conducted by three methods: 1) finite element analysis (FEA); 2) the virtual joint method (VJM), and 3) matrix structural analysis (MSA). One of the most reliable methods for stiffness analysis is FEA, because by this means, each link, joint, and actuator can be modelled with its actual shape; however, FEA is highly demanding in computation time, especially when used in optimization procedures. In [2] the stiffness of the H4 parallel robot was analyzed by FEA, at one single posture, the results having been verified experimentally. The second method, VJM, is based on the work first proposed by Gosselin [3]. In this method, which is sometimes called *lumped-parameter method*, the compliance of the links is replaced by virtual compliant joints and rigid links . Then, by virtue of the elastic properties of the model, the equivalent virtual joint stiffnesses are derived. In this way, complex relations in the stiffness analysis are avoided and acceptable accuracy in short computational times is possible; however, because of the one-dimensional virtual springs in the model, the coupling effect between translational and rotational deflections is not taken into account. Later, the VJM was applied to conduct the stiffness analysis of spatial six-degree-of-freedom (dof) parallel robots with revolute joints[4]. Majou et al. applied the VJM to the Orthoglide robot in order to establish a parametric representation of the Cartesian stiffness matrix [5]; however, coupling effects between translational and rotational deflections were neglected. Later, a modification was applied to the VJM in order to take into account the coupling in question [6]; this analysis was based on a multidimensional lumped-parameter model that replaces the link compliance with localized six-dof virtual springs. By this means the coupling between translational and rotational deflections was considered. To ensure high accuracy, the spring-stiffness values were calculated using FEA. The main idea behind the third method, MSA, is similar to FEA; however, instead of using a large number of elements, each part of the robot, link, joint, or actuator, is considered as a simple structural element, beam or rod, for example. By resorting to the theories of elasticity and kinematic chains, the stiffness matrix of the whole robot structure is obtained. The main issue that distinguishes MSA from other methods is that, within MSA, the stiffness matrix of the structure can be obtained in parametric form, which is important when the stiffness of the structure is to be optimized. Deblaise et al. found the Cartesian stiffness matrix of the Delta parallel structure

by using this method [7], while in [8] the MSA for the stiffness analysis of the 6-$\underline{\text{R}}$SS robot[1] was employed.

A novel method, based on the well-known concept of *generalized spring* [13], is proposed in this paper; this method relies mostly on a form of the MSA, but enhanced here with equivalent springs for the flexible parts, in serial and parallel arrays. The concept of generalized spring appears to have first been proposed by Lončarić [13] as a suspension for a rigid body and composed of single linearly elastic translational springs. By means of the method proposed here, the 6×6 Cartesian stiffness matrix of the robot, *for any robot posture*, can be calculated using stiffness matrices computed offline by means of FEA. Moreover, although the method is limited to linearly elastic structural elements, it is general enough to accommodate elastic anisotropies, as appearing in composite materials. The method is especially attractive in the realm of parallel robots with what is known as Π-joints, which are *parallelogram four-bar linkages* [10, 11]. The specific property of this joint, under the assumption that its links are all rigid, is that any two opposite links move under pure relative translation. Because of this property, Π joints are widely used in designing industrial parallel robots, e.g. ABB's Flexpicker and Adept's Quattro. By means of the generalized spring concept, the stiffness matrix of the Π joints can be readily calculated, as shown presently. An important issue arises when some robot parts are made either of composite materials, or with complex shapes. In such cases, the only reliable method of structural analysis would be FEA. As the stiffness matrix of a robot is posture-dependent, the elastostatic analysis on the whole workspace would be too time consuming to be practical. To cope with this problem, we propose a combination of FEA and the generalized spring concept. In this approach, by means of FEA the stiffness matrix of each complex part is calculated once and for all; then, the stiffness matrix thus obtained is used when computing the Cartesian stiffness matrix of the equivalent generalized spring at a given robot posture. Therefore, FEA is used only once, off-line, thereby saving precious computation time and analysis costs. The concept is illustrated with the calculation of the stiffness matrix of a two-limb Schönflies Motion Generator. As an illustrative example, the robot stiffness matrix is computed along a MP trajectory. It is expected that the procedure will enable the real-time stiffness control of robotic structures, thereby allowing for faster, more accurate and safer operations.

2 The Small-rotation Matrix

The rotation of a rigid body displaced from an initial attitude to a new one can be represented in a variety of forms. In this study the natural invariants of the rotation are used; these are the angle of rotation ϕ and the unit vector $\mathbf{e}$ parallel to the axis of rotation [9]. The rotation matrix is then represented as

$$\mathbf{R} = \mathbf{1} + (\sin\phi)\,\mathbf{E} + (1 - \cos\phi)\,\mathbf{E}^2 \tag{1}$$

with $\mathbf{E}$ denoting the cross-product matrix (CPM) of $\mathbf{e}$, which is defined for any three-dimensional vector $\mathbf{v}$ as

$$\mathbf{E} = \frac{\partial\,(\mathbf{e} \times \mathbf{v})}{\partial \mathbf{v}} \tag{2}$$

[1] $\underline{\text{R}}$ denotes an actuated revolute joint, while S stands for spherical, or ball-and-socket, joint.

and $\mathbf{1}$ is the 3×3 identity matrix. The angular velocity of the rigid body in terms of $\mathbf{e}$, ϕ and their time-derivative takes the form [9]

$$\boldsymbol{\omega} = \begin{bmatrix} (\sin\phi)\,\mathbf{1} + (1-\cos\phi)\,\mathbf{E} & \mathbf{e} \end{bmatrix} \begin{bmatrix} \dot{\mathbf{e}} \\ \dot{\phi} \end{bmatrix} \tag{3}$$

If ϕ is small, then $\sin\phi \to \phi$ and $\cos\phi \to 1$, the rotation matrix $\mathbf{R}$ thus becoming

$$\mathbf{R} = \mathbf{1} + \phi\mathbf{E} \tag{4}$$

Under the small-angle assumption, a rigid-body rotation admits a vector representation,

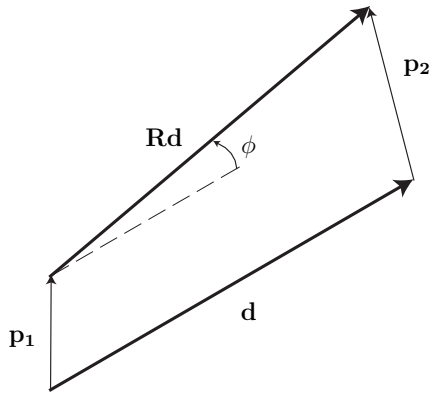

Figure 1: A vector attached to a rigid body after and before translation and small rotation

namely,

$$\boldsymbol{\phi} \equiv \phi\mathbf{e} \tag{5}$$

the angular velocity $\boldsymbol{\omega}$ for small ϕ then reducing to

$$\boldsymbol{\omega} = \begin{bmatrix} \phi\mathbf{1} & \mathbf{e} \end{bmatrix} \begin{bmatrix} \dot{\mathbf{e}} \\ \dot{\phi} \end{bmatrix}$$

i.e,

$$\boldsymbol{\omega} = \dot{\boldsymbol{\phi}} = \phi\dot{\mathbf{e}} + \dot{\phi}\mathbf{e}$$

In this particular case, the angular-velocity vector becomes a time-derivative. In Fig. 1 a vector $\mathbf{d}$ attached to a rigid body is shown before and after the body undergoes a small-amplitude displacement. The algebraic relations among the vectors of Fig. 1 lead to

$$\mathbf{p}_2 = \mathbf{p}_1 + (\mathbf{R} - \mathbf{1})\,\mathbf{d} \tag{6}$$

From eq. (4), after some algebraic manipulations,

$$\mathbf{p}_2 = \mathbf{p}_1 - \mathbf{D}\boldsymbol{\phi} \tag{7}$$

in which $\mathbf{D}$ is the cross product matrix of $\mathbf{d}$. Finally, the six-dimensional small displacement of two points of a rigid body becomes

$$\begin{bmatrix} \mathbf{p}_2 \\ \boldsymbol{\phi} \end{bmatrix} = \begin{bmatrix} \mathbf{1} & -\mathbf{D} \\ \mathbf{O} & \mathbf{1} \end{bmatrix} \begin{bmatrix} \mathbf{p}_1 \\ \boldsymbol{\phi} \end{bmatrix} \tag{8}$$

where $\mathbf{O}$ is the 3×3 zero matrix. Moreover, the six-dimensional SAD $\mathbf{u}_i$, for $i = 1, 2$, is defined as

$$\mathbf{u}_i = \begin{bmatrix} \mathbf{p}_i \\ \boldsymbol{\phi} \end{bmatrix} \tag{9}$$

3 Generalized Spring

In multibody systems some flexible links are rigidly connected to each other or to other much stiffer bodies that can be safely assumed rigid. The main source of potential energy is the elastic energy stored in the former. Each of these can be considered a generalized six-dimensional massless spring with one end undergoing six-dimensional SADs $\mathbf{u}$. We label the first and the second ends constrained and free end, respectively, which is shown in Fig. 2. In this definition, the ends are considered to be rigid plates, on which a force $\mathbf{f}$ and a moment $\mathbf{n}$, grouped in the six-dimensional wrench array $\mathbf{w}$ [9] can be applied. The wrench is the image of the displacement vector $\mathbf{u}$ under a transformation represented by the Cartesian 6×6 stiffness matrix $\mathbf{K}$, namely,

$$\mathbf{w} = \mathbf{K}\mathbf{u} \tag{10}$$

In the especial case in which all six possible motions of the first end are constrained, the matrix $\mathbf{K}$ is positive-definite. The rank $r(\mathbf{K})$ of the matrix $\mathbf{K}$ generally depends on the number of constraints imposed on the first end. The dimension of the null space of the

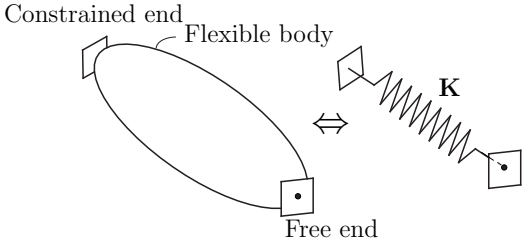

Figure 2: A generalized spring

matrix $\mathbf{K}$ represents the number of independent rigid-body motions that the free end can undergo without producing any potential energy in the spring.

3.1 The Equivalent Generalized Spring in Multibody Systems

A mechanical system is composed of some flexible bodies, which are connected by means of joints. To calculate the stiffness matrix of a mechanical system it is convenient to represent its flexible elements with six-dimensional generalized springs; then, two or more springs are

replaced with one equivalent single spring. Two possible arrays occur: parallel and serial, as shown in Figs. 3(a) and (b), respectively. The equivalent spring for the parallel and serial arrays is defined as the single spring that stores the same potential energy as the two springs combined, under the same relative SAD of the two end-plates. The stiffness matrix of the equivalent single spring of the parallel array is calculated from the potential energy of the system:

$$V = \frac{1}{2}\left(\mathbf{u}_2^T\mathbf{K}_1\mathbf{u}_2 + \mathbf{u}_4^T\mathbf{K}_2\mathbf{u}_4\right) \tag{11}$$

Upon resorting to eq. (8) the relations between the displacement vectors of the nodes on the rigid bodies are

$$\mathbf{u}_2 = \begin{bmatrix}\mathbf{1} & -\mathbf{A}_1\\ \mathbf{O} & \mathbf{1}\end{bmatrix}\mathbf{u}_{O1} \equiv \mathbf{W}_1\mathbf{u}_{O1}, \quad \mathbf{u}_4 = \begin{bmatrix}\mathbf{1} & -\mathbf{A}_2\\ \mathbf{O} & \mathbf{1}\end{bmatrix}\mathbf{u}_{O1} \equiv \mathbf{W}_2\mathbf{u}_{O1} \tag{12}$$

in which $\mathbf{A}_1$ and $\mathbf{A}_2$ are the cross product matrices of vectors $\mathbf{a}_1$ and $\mathbf{a}_2$, respectively; $\mathbf{O}$ is the 3×3 zero matrix and $\mathbf{1}$ is the 3×3 identity matrix. Moreover, $\mathbf{u}_{O2}$ is the SAD of the free end O_2 of the equivalent single spring. Upon substitution of the above expression into eq. (11), one obtains

$$V = \frac{1}{2}\mathbf{u}_{o2}^T\left(\mathbf{W}_2^T\mathbf{K}_1\mathbf{W}_2 + \mathbf{W}_4^T\mathbf{K}_2\mathbf{W}_4\right)\mathbf{u}_{o2} \tag{13}$$

Knowing that the derivative of the potential energy with respect to the displacement vector of the free end at a given point equals the wrench applied at that point,

$$\frac{\partial V}{\partial \mathbf{u}} = \mathbf{w} \tag{14}$$

whence,

$$\frac{\partial V}{\partial \mathbf{u}_{o2}} = \mathbf{w} = \left(\mathbf{W}_2^T\mathbf{K}_1\mathbf{W}_2 + \mathbf{W}_4^T\mathbf{K}_2\mathbf{W}_4\right)\mathbf{u}_{o2} \tag{15}$$

From eq. (15) the stiffness matrix of the equivalent single spring, mapping the free-end displacement vector onto the wrench applied on that end, is simply the coefficient matrix in eq. (15), namely,

$$\mathbf{K}^{\mathrm{Par}} = \mathbf{W}_1^T\mathbf{K}_1\mathbf{W}_1 + \mathbf{W}_2^T\mathbf{K}_2\mathbf{W}_2 \tag{16}$$

For the serial array, depicted in Fig. 3(b), the same procedure is applicable. As shown in the same figure, two serial six-dimensional springs in series are replaced with its single equivalent. The potential energy of the system is

$$V = \frac{1}{2}\left[\mathbf{u}_2^T\mathbf{K}_1\mathbf{u}_2 + \left(\mathbf{u}_4 - \mathbf{u}_3\right)^T\mathbf{K}_2\left(\mathbf{u}_4 - \mathbf{u}_3\right)\right] \tag{17}$$

As in the case of parallel springs, the relations between the displacement vectors are

$$\begin{gathered}\mathbf{u}_2 = \begin{bmatrix}\mathbf{1} & -\mathbf{A}_1\\ \mathbf{O} & \mathbf{1}\end{bmatrix}\mathbf{u}_{O2} \equiv \mathbf{W}_1\mathbf{u}_{O2}, \quad \mathbf{u}_3 = \begin{bmatrix}\mathbf{1} & -\mathbf{A}_2\\ \mathbf{O} & \mathbf{1}\end{bmatrix}\mathbf{u}_{O2} \equiv \mathbf{W}_2\mathbf{u}_{O2}\\ \mathbf{u}_4 = \begin{bmatrix}\mathbf{1} & -\mathbf{A}_3\\ \mathbf{O} & \mathbf{1}\end{bmatrix}\mathbf{u}_{O3} \equiv \mathbf{W}_3\mathbf{u}_{O3}\end{gathered} \tag{18}$$

Upon substitution of eq. (18) into eq. (17), the potential energy is obtained in terms of the displacement vectors, $\mathbf{u}_{o1}$, $\mathbf{u}_{o2}$ and $\mathbf{u}_{o3}$. For the sake of brevity, the final force-displacement relation is shown, without the intermediate steps:

$$\mathbf{w}_2 = \mathbf{W}_1^T\mathbf{K}_1\mathbf{W}_1\mathbf{u}_{O1} + \mathbf{W}_2^T\mathbf{K}_2\mathbf{W}_3\mathbf{u}_{O2} \tag{19a}$$

$$\mathbf{w}_3 = \mathbf{W}_3^T\mathbf{K}_2\mathbf{W}_2\mathbf{u}_{O1} + (\mathbf{W}_1^T\mathbf{K}_1\mathbf{W}_1 + \mathbf{W}_2^T\mathbf{K}_2\mathbf{W}_2)\mathbf{u}_{O2} \tag{19b}$$

where $\mathbf{O}$ is the 3×3 zero matrix, and $\mathbf{0}$ is the three-dimensional zero vector. Here, the mapping between the SAD $\mathbf{u}_{O3}$ and the applied wrench $\mathbf{w}_{O3}$ is required; it is assumed that $\mathbf{w}_3 = \mathbf{0}$. Under this assumption, eq. (19b) enables us to calculate $\mathbf{u}_{O3}$ in terms of $\mathbf{u}_{O2}$, namely,

$$\mathbf{u}_{O3} = -\mathbf{P}^{-1}\mathbf{W}_3^T\mathbf{K}_2\mathbf{W}_2\mathbf{u}_{O2} \tag{20}$$

with $\mathbf{P}$ defined as

$$\mathbf{P} = \mathbf{W}_2^T\mathbf{K}_2\mathbf{W}_2 + \mathbf{W}_1^T\mathbf{K}_1\mathbf{W}_1 \tag{21}$$

Upon substitution of eq. (20) into eq. (19a), the matrix mapping the SAD $\mathbf{u}_{O2}$ into the wrench $\mathbf{w}_2$ is obtained as

$$\mathbf{K}^{\text{ser}} = \mathbf{W}_3^T\mathbf{K}_2\mathbf{W}_3 - \mathbf{W}_3^T\mathbf{K}_2\mathbf{W}_2\mathbf{P}^{-1}\mathbf{W}_2^T\mathbf{K}_2\mathbf{W}_3 \tag{22}$$

which is the equivalent stiffness matrix of the serial array. It is apparent from expressions (16)

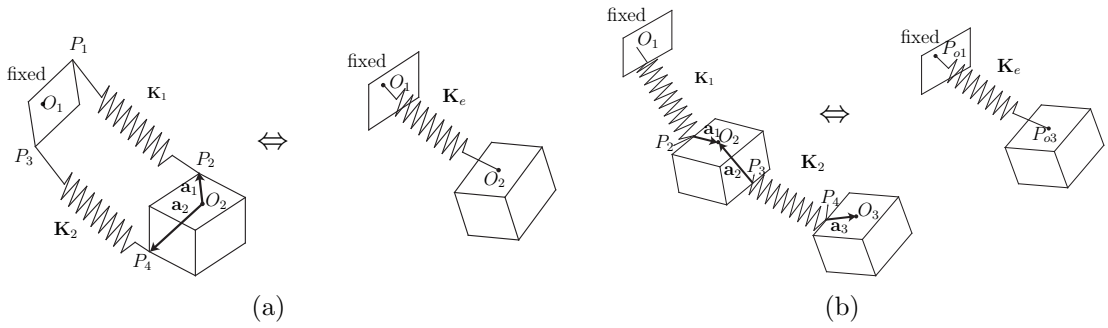

Figure 3: Generalized equivalent spring of: (a) two parallel springs and (b) two serial springs

and (22) that, once $\mathbf{K}_1$ and $\mathbf{K}_2$ are available, with as high a level of realism and accuracy as needed, the updating of the parallel and serial equivalent stiffness matrices follows with a negligible computational cost. Indeed the multiplication of two 6×6 matrices includes 36 scalar products of two six-dimensional vectors; this multiplication thus needs $6 \times 36 = 216$ flops. At each posture, the calculation of a parallel array stiffness matrix include four multiplications of 6×6 matrices, which results in 864 flops. In the case of serial arrays there are 10 multiplications plus the inversion of a 6×6 matrix, which needs $6 \times 127 = 762$ flops; therefore, to calculate the stiffness matrix of a serial array $2160 + 762 = 2922$ flops are required. The effect of passive revolute joints, always present in parallel robots, is discussed below.

3.2 A Flexible Body Coupled by Means of Passive Revolute Joints

Assume that the first end of the flexible body is attached to the previous body via a passive revolute joint R, as depicted in Fig. 4. This joint allows the flexible link to freely rotate about axis $\mathcal{A}$, which means that, if a force is applied at the free end of the flexible body in a direction normal to $\mathcal{A}$, the potential energy of the spring does not change. In other words, a link with a revolute joint exhibits a zero translational stiffness along the line of action of the force, which reduces the rank of the stiffness matrix by one.

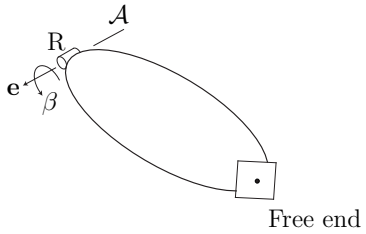

Figure 4: A link with passive revolute joint

3.3 Stiffness Matrix of the Π-joint

In the Π-joint shown in Fig. 5, the two shorter links are assumed rigid, the flexibility of the Π-joint coming from the two identical longer links, which are articulated to the rigid links by means of R joints of parallel axes. Therefore, the Π joint can be modelled as a parallel array of two equivalent generalized springs of the two articulated flexible links. The stiffness matrix $\mathbf{K}_l$ of each of the two foregoing links, which is the positive-semidefinite equivalent stiffness matrix of each of the links with one passive revolute joint at the first end, is first calculated. Then, the stiffness of the equivalent spring of the Π joint becomes

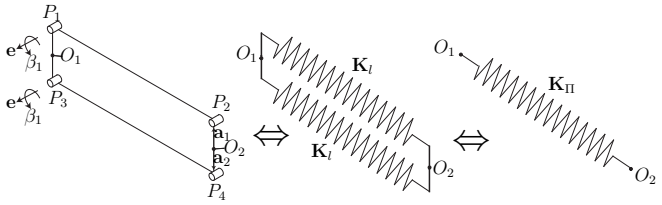

Figure 5: Equivalent single spring for the Π-joint

$$\mathbf{K}^{\Pi} = \mathbf{W}_1^T \mathbf{K}_l \mathbf{W}_1 + \mathbf{W}_2^T \mathbf{K}_l \mathbf{W}_2 \tag{23}$$

It is noteworthy that O_1 and O_2 can be any arbitrary points of the rigid bodies; for modal analysis, the centre of mass of each rigid body is the best candidate. The flexible links of the Π-joint can be made of any linearly elastic material and with any shape; in some cases, for example, when the Π joints are made of composite materials with complex shapes, it is not possible to have the stiffness matrix $\mathbf{K}_l$ of the link in parametric form. The stiffness matrix must then be calculated numerically, using, e.g., FEA; the stiffness matrix of the

Π joint is obtained from eq. (23) once matrix $\mathbf{K}_l$ is available from a FEA. This procedure, which can be used for any other flexible parts, yields the general posture-dependent stiffness matrix of a flexible component. The foregoing computations can be done online, as shown in Subsection 3.1

4 Case Study: The McGill SMG

The foregoing results are used to calculate the stiffness matrix of the McGill Schönflies Motion Generator, shown in Fig. 6, which is modelled as the elastostatic system depicted in Fig. 7. Kinetostatically, each limb consists of three rigid links: the base platform (BP), the elbow brackets, and the wrist bracket. Each limb couples, moreover, the MP with the BP. The parallelograms are thus regarded as joints, namely, Π joints. The kinematic chain of the McGill SMG is thus of the RΠΠΠRRΠΠΠR type. The kinematic chain thus contains eight rigid links and eight joints, with dof = 4. In this model each Π-joint is replaced with the corresponding equivalent six-dimensional generalized spring. The McGill SMG has two

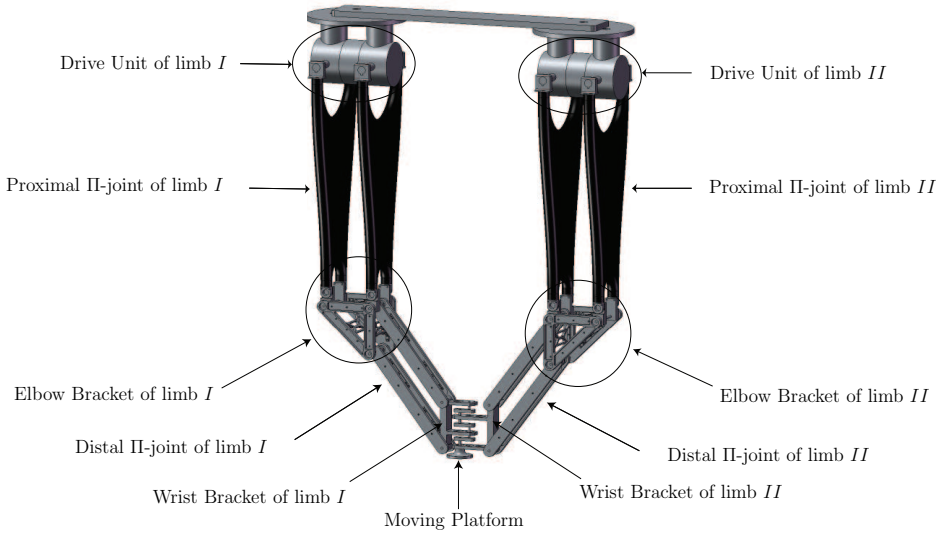

Figure 6: The McGill SMG

kinds of Π-joints, proximal and distal, as depicted in Fig. 6. Each distal Π-joint is made of two identical aluminium rods, which are modeled as flexible beams; the stiffness of the equivalent single spring can then be obtained by means of the beam stiffness matrix, which is shown below,

$$\mathbf{K} = \frac{E}{L}\begin{bmatrix} A & 0 & 0 & 0 & 0 & 0 \\ 0 & 12I_z/L^2 & 0 & 0 & 0 & 6I_z/L \\ 0 & 0 & 012I_y/L^2 & 0 & -6I_y/L & 0 \\ 0 & 0 & 0 & JG/E & 0 & 0 \\ 0 & 0 & -6I_y/L & 0 & 4I_y & 0 \\ 0 & 6I_z/L & 0 & 0 & 0 & 4I_z \end{bmatrix} \tag{24}$$

In the case of the proximal Π-joints, these include two boxes made of a combination of woven and unidirectional carbon/epoxy material, for which no closed-form parametric stiffness matrix is available. Because of the complex shape and the complexity associated with the modelling of composite materials, finite element software (ANSYS) was used to calculate the stiffness matrix of the composite box. ANSYS provides an option in the solution processor, called Substructure, in which the Cartesian stiffness matrix of a structure can be obtained. Now the equivalent stiffness matrices of the proximal and distal Π joints, labeled $\mathbf{K}_P$ and $\mathbf{K}_D$, respectively, are calculated via eq. (23). In the ensuing elastostatic analysis we assume that the rigid bodies are massless, and thus, when the springs are in a serial array, as explained in Section 3.1, the series equivalent single spring is used. As depicted in Fig. 7, each robot limb is considered a serial array of two springs, which is then simplified to the equivalent single spring for each limb in the elastostatic analysis. By resorting to eq.(22), the equivalent stiffness of limb J, for $J = I, II$, is

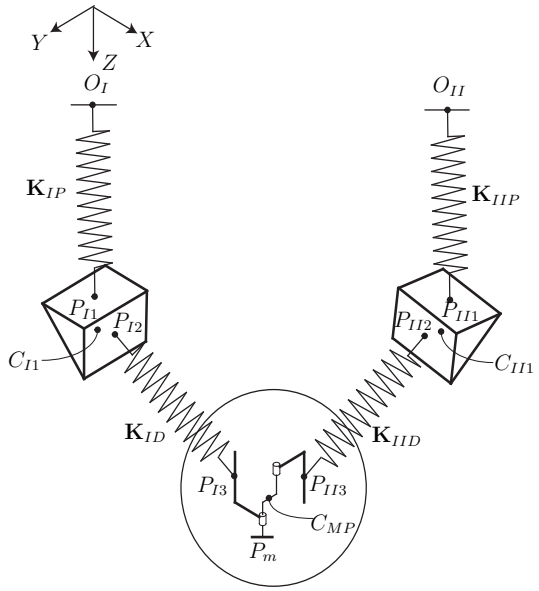

Figure 7: Elastostatic model of the McGill SMG

$$\mathbf{K}_J = \mathbf{W}_{J3}^T \mathbf{K}_{JD} \mathbf{W}_{J3} - \mathbf{W}_{J3}^T \mathbf{K}_{JD} \mathbf{W}_{J2} \mathbf{P}_J^{-1} \mathbf{W}_{J2}^T \mathbf{K}_{JD} \mathbf{W}_{J3} \tag{25}$$

where $\mathbf{K}_{JD}$ denotes the stiffness matrix of the distal Π joint of limb J, and

$$\mathbf{P}_J = \mathbf{W}_{J2}^T \mathbf{K}_{JD} \mathbf{W}_{J2} + \mathbf{W}_{J1}^T \mathbf{K}_{JP} \mathbf{W}_{J1}$$

with $\mathbf{K}_{JP}$ denoting the stiffness matrix of the proximal Π joint of limb J. The equivalent single spring of each limb is connected to its wrist brackets as depicted in Figs. 6 and 7, and zoom-in in Fig. 8. The two wrist brackets are connected, in turn, to the MP by means of revolute joints; hence, by invoking the rigidity assumption and because of the presence of the revolute joints, we have

$$\mathbf{u}_{J3} = \mathbf{G}_J(\mathbf{H}_J \mathbf{u}_m + \gamma_J \boldsymbol{\zeta}), \quad \boldsymbol{\zeta} = \begin{bmatrix} \mathbf{0}^T & \mathbf{e}_\gamma^T \end{bmatrix}^T \tag{26}$$

in which $\mathbf{0}$ is the three-dimensional zero vector, and $\mathbf{e}_\gamma$ is the unit vector parallel to the revolute joint axis, which, in this case, is $\begin{bmatrix}0 & 0 & 1\end{bmatrix}^T$, and hence, constant. Moreover,

$$\mathbf{G}_J = \begin{bmatrix}\mathbf{1} & -\mathbf{A}_J \\ \mathbf{0} & \mathbf{1}\end{bmatrix}, \quad \mathbf{H}_J = \begin{bmatrix}\mathbf{1} & -\mathbf{D}_J \\ \mathbf{0} & \mathbf{1}\end{bmatrix} \tag{27}$$

where $\mathbf{A}_J$ and $\mathbf{D}_J$ are the cross-product matrices of vectors $\mathbf{a}_J$ and $\mathbf{d}_J$, respectively, for $J = I, II$, and depicted in Fig. 8. From eq. (26) the potential energy of the robot is

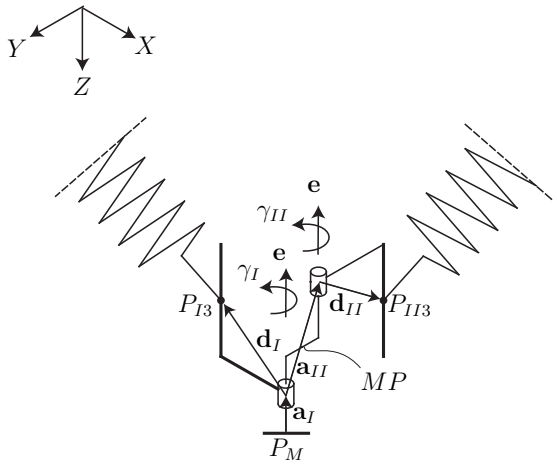

Figure 8: A zoom-in of the MP and the wrist brackets in the elastostatic model of the McGill SMG

calculated as

$$V = \frac{1}{2}\sum_{J=I,II} \mathbf{u}_J^T \mathbf{K}_J \mathbf{u}_J, \quad \mathbf{u}_J = \mathbf{G}_J(\mathbf{H}_J\mathbf{u}_m + \gamma_J\boldsymbol{\zeta}), \quad J = I, II \tag{28}$$

Given that the passive revolute joints transmit a zero moment about their axes, the angle of rotation γ_J can be found in terms of $\mathbf{u}_M$, the six-dimensional displacement vector of the MP at point P_M, as

$$\gamma_J = \mathbf{v}_J^T \mathbf{u}_M \tag{29}$$

where the six-dimensional vector $\mathbf{v}_J$ is defined as

$$\mathbf{v}_J = -\frac{1}{\boldsymbol{\zeta}^T\mathbf{G}_J\mathbf{K}_J\mathbf{G}\boldsymbol{\zeta}}\mathbf{H}_J^T\mathbf{G}^T\mathbf{K}_J\mathbf{G}_J\boldsymbol{\zeta}$$

Upon substitution of eq. (29) into eq. (28), the 6×6 stiffness matrix of the overall robot becomes, finally,

$$\mathbf{K} = \sum_{J=I,II} \left(\mathbf{G}_J\mathbf{H}_J + \mathbf{G}_J\boldsymbol{\zeta}\mathbf{v}_J^T\right)^T \mathbf{K}_J \left(\mathbf{G}_J\mathbf{H}_J + \mathbf{G}_J\boldsymbol{\zeta}\mathbf{v}_J^T\right) \tag{30}$$

which relates the SAD of the MP, defined at point P_M, to the wrench applied onto the MP, with force acting along a line that passes through P_M.

5 Stiffness Indices

In order to assess the elastostatic response of a robot to an external wrench, defining stiffness indices is essential. Here, the main issue is that a 6×6 Cartesian stiffness matrix is formed by four 3×3 block matrices whose components have different units, which is made apparent below:

$$\begin{bmatrix} \mathbf{f} \\ \mathbf{n} \end{bmatrix} = \begin{bmatrix} \mathbf{K}_{11}(\mathrm{N/m}) & \mathbf{K}_{12}(\mathrm{N}) \\ \mathbf{K}_{12}^T(\mathrm{N}) & \mathbf{K}_{22}(\mathrm{N.m}) \end{bmatrix} \begin{bmatrix} \mathbf{s} \\ \boldsymbol{\theta} \end{bmatrix} \tag{31}$$

where $\mathbf{f}$ and $\mathbf{n}$ denote force and moment, respectively, the six dimensional array of the left-hand side being a wrench; $\mathbf{s}$ and $\boldsymbol{\theta}$ define, in turn, a "small" point-translation—small with respect to the dimensions of the system bodies—and a "small" rotation about an axis parallel to the unit vector $\boldsymbol{\theta}/\left\|\boldsymbol{\theta}\right\|$, respectively. The six-dimensional array of the right-hand side is thus a "small"-amplitude rigid-body displacement. To define stiffness performance indices, first we should nondimensionalize the stiffness matrix. The method used here is based on the idea introduced in [14], to define dimensionless parameters for sensitivity analysis of mechanical systems. The two equations (31), one for moment and one for force, are displayed below:

$$\mathbf{f} = \mathbf{K}_{11}\mathbf{s} + \mathbf{K}_{12}\boldsymbol{\theta} \tag{32a}$$

$$\mathbf{n} = \mathbf{K}_{12}^T\mathbf{s} + \mathbf{K}_{22}\boldsymbol{\theta} \tag{32b}$$

Apparently, the force and moment vectors are made up of two independent components, namely,

$$\mathbf{f} = \mathbf{K}_{11}\mathbf{s} + \mathbf{K}_{12}\boldsymbol{\theta} = \mathbf{f}_s + \mathbf{f}_\theta \tag{33a}$$

$$\mathbf{n} = \mathbf{K}_{12}^T\mathbf{s} + \mathbf{K}_{22}\boldsymbol{\theta} = \mathbf{n}_s + \mathbf{n}_\theta \tag{33b}$$

We can associate each independent part of eqs. (33a) and (33b) with a physically meaningful quadratic form [14], such as $\left\|\mathbf{f}_\beta\right\|^2 = \boldsymbol{\beta}^T\mathbf{K}_{\boldsymbol{\beta}}^T\mathbf{K}_{\boldsymbol{\beta}}\boldsymbol{\beta}$, which defines an ellipsoid in the space of $\boldsymbol{\beta}$, a dummy vector variable, to be defined presently for $\boldsymbol{\beta} = \mathbf{s}$, a point-displacement, and $\boldsymbol{\beta} = \boldsymbol{\theta}$, a "small"-angle rotation vector, similar to $\boldsymbol{\phi}$ of eq. (5). The eigenvalues of $\mathbf{K}_{\boldsymbol{\beta}}^T\mathbf{K}_{\boldsymbol{\beta}}$ are then used to define dimensionless parameters. A relation between two dimensionless parameter vectors $\mathbf{p}_\beta$ and $\boldsymbol{\beta}$ is now introduced:

$$\boldsymbol{\beta} = \mathbf{S}_\beta\mathbf{p}_\beta \tag{34}$$

where $\mathbf{S}_\beta$ is an orthogonal matrix whose columns are the eigenvectors of matrix $\mathbf{K}_\beta^T\mathbf{K}_\beta$. In our case, to define dimensionless parametrs we will have two linear transformation regarding the force and moment equations; for the force equation the linear transformation leads to

$$\begin{bmatrix} \mathbf{s} \\ \boldsymbol{\theta} \end{bmatrix} = \begin{bmatrix} \mathbf{S}_s & \mathbf{O} \\ \mathbf{O} & \mathbf{S}_\theta \end{bmatrix} \begin{bmatrix} \boldsymbol{\psi}_s \\ \boldsymbol{\psi}_\theta \end{bmatrix} \tag{35}$$

while, for the moment equation,

$$\begin{bmatrix} \mathbf{s} \\ \boldsymbol{\theta} \end{bmatrix} = \begin{bmatrix} \mathbf{H}_s & \mathbf{O} \\ \mathbf{O} & \mathbf{H}_\theta \end{bmatrix} \begin{bmatrix} \boldsymbol{\nu}_s \\ \boldsymbol{\nu}_\theta \end{bmatrix} \tag{36}$$

Thus, by substitution of eqs.(35) and (36) into eqs.(32a) and (32b), respectively, the force and moment vectors are transformed into dimensionless parameter vectors by means of new linear transformations,

$$\mathbf{f} = \mathbf{G}_f \boldsymbol{\psi}, \quad \mathbf{n} = \mathbf{G}_n \boldsymbol{\nu} \tag{37}$$

in which $\mathbf{G}_f$ and $\mathbf{G}_n$ are unit-homogenized coefficient matrices that have units corresponding to $\mathbf{f}$ and $\mathbf{n}$, respectively, i.e.,

$$\begin{aligned} \mathbf{G}_f &= \begin{bmatrix} \mathbf{K}_{11}\mathbf{S}_s & \mathbf{K}_{12}\mathbf{S}_\theta \end{bmatrix}, \quad \boldsymbol{\psi} = \begin{bmatrix} \boldsymbol{\psi}_s^T & \boldsymbol{\psi}_\theta^T \end{bmatrix}^T \\ \mathbf{G}_n &= \begin{bmatrix} \mathbf{K}_{12}^T\mathbf{H}_s & \mathbf{K}_{22}\mathbf{H}_\theta \end{bmatrix}, \quad \boldsymbol{\nu} = \begin{bmatrix} \boldsymbol{\nu}_s^T & \boldsymbol{\nu}_\theta^T \end{bmatrix}^T \end{aligned} \tag{38}$$

Matrix $\mathbf{G}_f^T\mathbf{G}_f$ has three independent eigenvectors corresponding to three eigenvalues that characterize the distorted unit sphere $\|\mathbf{f}\|^2 = 1$. The eigenvalues and eigenvectors of $\mathbf{G}_n^T\mathbf{G}_n$ entail a similar interpretation. $\mathbf{G}_f^T\mathbf{G}_f$ has three mutually orthogonal eigenvectors corresponding to three non-negative eigenvalues that charactrizes the distorsion of the unit sphere $\|\mathbf{f}\|$. By the same token, the eigenvalues and eigenvectors of $\mathbf{G}_n^T\mathbf{G}_n$ yield an ellipsoid in the nondimensional space of $\boldsymbol{\nu}$. The mean values of the eigenvalues of $\mathbf{G}_f^T\mathbf{G}_f$ and $\mathbf{G}_m^T\mathbf{G}_m$, $\{\lambda_i^f\}_1^3$ and $\{\lambda_i^m\}_1^3$, respectively, are now defined as translational κ_t and rotational κ_r stiffness performance indices, respectively, i.e.,

$$\kappa_t = \sqrt{\frac{1}{3}\sum_{i=1}^{3}\lambda_i^f}, \quad \kappa_r = \sqrt{\frac{1}{3}\sum_{i=1}^{3}\lambda_i^m} \tag{39}$$

where the square roots have been introduced because of the quadratic nature of $\mathbf{G}_f^T\mathbf{G}_f$ and $\mathbf{G}_m^T\mathbf{G}_m$.

5.1 Numerical Results

Now we compute the stiffness performance indices of the McGill SMG while going through a pick-and-place operation following a standard test trajectory, which involves a 25 mm vertical upward translation, a 300 mm horizontal translation, and a 25 mm downward vertical translation. Moreover, the MP should follow this trajectory with a rotation of 180° while moving along the horizontal segment. Here, we use the smoothed test trajectory reported by Gauthier et al. [15], which is depicted in Fig. 9. The translational and rotational stiffness indices of the McGill SMG through the test trajectory are shown in Fig. 10. The behaviour of the two performance indices through the trajectory shows the points at which the robot has poor stiffness: the higher the index, the stiffer the structure. However, indices can be used either for assessment of the behaviour of the robot at different points of the trajectory or for design optimization purposes, but the two stiffness indices help the designer analyze the stiffness of the structure accurately and much more in detail.

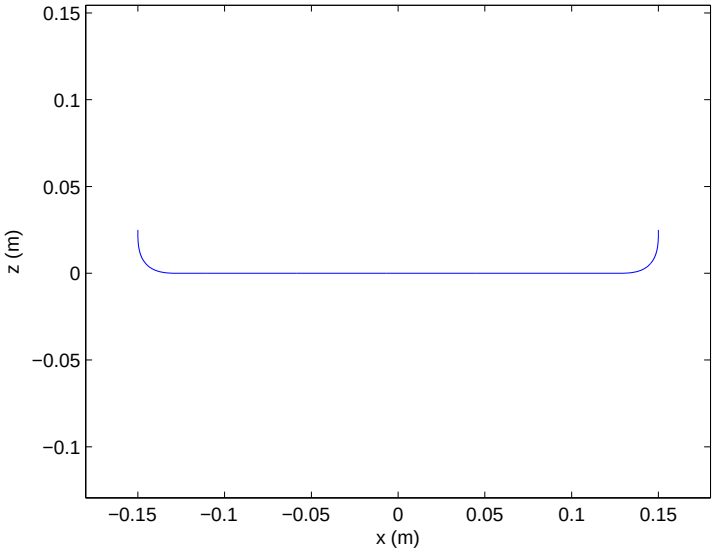

Figure 9: The smoothed test trajectory obtained in [15]

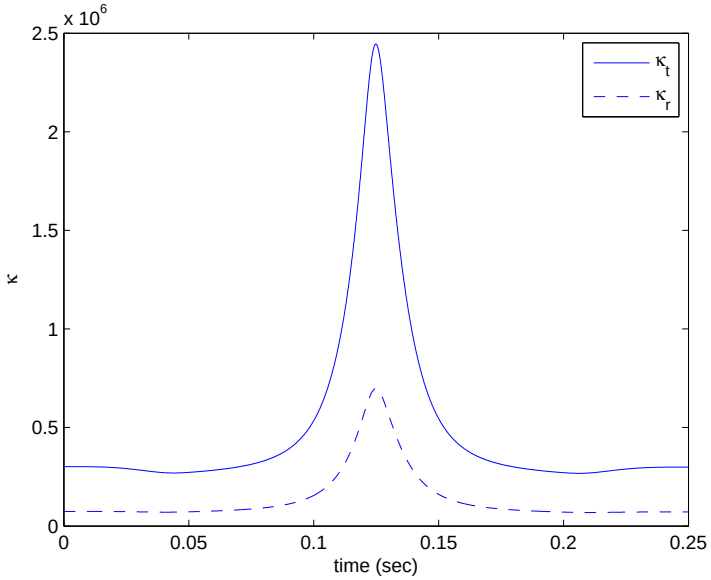

Figure 10: The general translational and rotational stiffness indices through the smoothed test trajectory

6 Conclusions

We proposed a method by which the stiffness matrix of complex robotic structures can be calculated by means of FEA conducted off-line. This provides substantial savings in time and calculation cost when the stiffness of the robot is to be calculated along a continuous trajectory. As a case study, the posture-dependent Cartesian stiffness matrix of the McGill SMG was computed. Furthermore, by means of a nondimensionalization of the stiffness matrix, two stiffness performance indices, translational and rotational, were introduced. These indices were computed along a standard test trajectory for the above-mentioned robot.

References

[1] H. Pottmann, and J. Wallner, *Computational Line Geometry*, Springer, Berlin-Heidelberg-New York, 2001.

[2] C. Corradini, J.C. Fauroux, S. Krut, O. Company, 'Evaluation of a 4-Degree of Freedom Parallel Manipulator Stiffness', *11th World Congress in Mechanism and Machine Science*, China, August 18-21, 2003.

[3] C.M. Gosselin, Stiffness mapping for parallel manipulator, *IEEE Trans. on Robotics and Automation*, vol. 6, 1990, pp. 377–382.

[4] C. Gosselin and D. Zhang, Stiffness Analysis of Parallel Mechanisms using a Lumped Model, *Int. Journal of Robotics and Automation*, vol. 17, 2002, pp. 17–27.

[5] F. Majou, C. Gosselin, P. Wenger, and D. Chablat, Parametric stiffness analysis of the Orthoglide, *Mechanism and Machine Theory*, vol. 42, 2007, pp. 296–311.

[6] A. Pashkevich and D. Chablat, 'Stiffness Analysis of Multi-Chain Parallel Robotic systems', *9th IFAC Workshop on Intelligent Manufacturing Systems*, Szczecin, Poland, October 9–10, 2008.

[7] D. Deblaise, X. Hernot and P. Maurine, 'A Systematic Analytical Method for PKM Stiffness Matrix Calculation', *IEEE International Conference on Robotics and Automation*, Orlando, USA, May 15–19, 2006.

[8] R. Sales Gonalves and J.C. Mendes Carvalho, 'Stiffness Analysis of Parallel Manipulator Using Matrix Structural Analysis', *Second European Conference on Mechanism Science*, Cassino, Italy, September 17–20, 2008.

[9] J. Angeles, *Fundamentals of Robotic Mechanical Systems Theory, Methods, and Algorithms*, Springer, 2007.

[10] J. Hervé and F. Sparacino, 'Star, a New Concept in Robotics', *Third Int. Workshop on Advances in Robot Kinematics*, Ferara, Italy, .

[11] K. Wohlhart, 'Displacement analysis of the general spatial parallelogram manipulator', *Third Int. Workshop on Advances in Robot Kinematics*, Ferara, Italy, September 7–9, 1992.

[12] A. Morozov, and J. Angeles, The mechanical design of a novel Schönflies Motion Generator, *Robotics and Computer-Integrated Manufacturing*, vol. 23, 2007, pp 82-93.

[13] J. Lončarić, The normal forms of a stiffness matrix and compliance matrices, *IEEE Journal of Robotics and Automation*, vol. RA-3, 1987, pp. 567–572.

[14] J. Kövecses, and S. Ebrahimi, Parameter Analysis and Normalization for the Dynamics and Design of Multibody Systems, *Journal of Computational and Nonlinear Dynamics* vol. 4, 2009.

[15] J.-F. Gauthier, J. Angeles, and S. Nokleby, Optimization of a Test Trajectory for SCARA Systems, *Advances in Robot Kinematics: Analysis and Design*, vol. 4, pp. 225–234.